Title page

Title

Shaping information processing: the role of oscillatory dynamics in a working-memory task

Author names & Affiliations

Hesham A. ElShafei[1], Ying Joey Zhou[1], Saskia Haegens[1,2,3]

[1] Donders Institute for Brain, Cognition & Behavior, Radboud University, Nijmegen, The Netherlands
[2] Dept. of Psychiatry, Columbia University, New York, NY, USA.
[3] Div. of Systems Neuroscience, New York State Psychiatric Institute, New York, NY, USA.

Corresponding author's name, email and postal address

Hesham A. ElShafei, elshafeh@gmail.com

Donders Institute for Brain, Cognition and Behaviour
Centre for Cognitive Neuroimaging
Radboud University Nijmegen
P.O. Box 9101
6500 HB Nijmegen
The Netherlands

Abstract

Neural oscillations are thought to reflect low-level operations that can be employed for higher-level cognitive functions. Here, we investigated the role of brain rhythms in the 1–30 Hz range by recording MEG in participants performing a visual delayed match-to-sample paradigm in which orientation or spatial frequency of sample and probe gratings had to be matched. A cue occurring before or after sample presentation indicated the to-be-matched feature. We demonstrate that alpha/beta power decrease tracks the presentation of the informative cue and indexes faster responses. Moreover, these faster responses coincided with an augmented phase alignment of slow oscillations, as well as phase-amplitude coupling between slow and fast oscillations. Importantly, stimulus decodability was boosted by both low alpha power and high beta power. In summary, we provide support for a comprehensive framework in which different rhythms play specific roles: slow rhythms control input sampling, while alpha (and beta) gates the information flow, beta recruits task-relevant circuits, and the timing of faster oscillations is controlled by slower ones.

Keywords

alpha rhythm; beta rhythm; MEG; brain oscillations; working memory

Highlights

- We test a comprehensive framework of rhythms as building blocks for information processing
- Participants performed a visual delayed match-to-sample task with pre- & retro-cues
- Phase alignment of slow rhythms, governing input sampling, indexes faster responses
- Alpha/beta power, gating information flow, boost behavior & track informative cues
- Low alpha (gating) & high beta (circuit-setup) power boost signal information content

1   Introduction

Brain oscillations reflect rhythmic fluctuations of neuronal ensembles between states of low and high excitability (Bishop, 1932). Earlier research primarily focused on investigating different oscillations independently and linking them to various high-level cognitive processes (e.g., theta to memory, alpha to attention). However, this approach might ultimately have limited explanatory power as the list of cognitive processes associated with particular oscillations is seemingly endless and, at this point, largely overlapping. Rather, the exact functional role of each rhythm likely depends on a dynamic interplay between brain region, underlying neuronal substrate, and task context (Buzsaki, 2006; Wang, 2010). Our working hypothesis is that brain oscillations reflect low-level mechanisms, rather than high-level cognitive functions, that can be flexibly employed to change the dynamics of neuronal populations, thereby providing the scaffolding for information processing. In this view, oscillations set the state of the system, either enhancing or attenuating activity (Klimesch et al., 2007), and inhibiting or facilitating network formation (Singer, 1999; Varela et al., 2001). Here we focus on oscillations in the delta/theta (1–7 Hz), alpha (8–14 Hz), and beta bands (15–30 Hz) in the context of a working-memory task.

Slow rhythms in the delta-to-theta bands have been proposed to govern the sampling of our surroundings by providing alternating phases of high and low neural excitability and thereby phases of high and low perceptual sensitivity (Fiebelkorn & Kastner, 2018; Helfrich et al., 2019; Herbst & Landau, 2016; VanRullen, 2016). In this view, sensory processing (and subsequent behavior) depends on the temporal coincidence of task relevant targets with the phase of ongoing oscillations; i.e., when the oscillatory phase with high excitability coincides with the occurrence of a target stimulus, neural and behavioral responses are enhanced (Busch et al., 2009; Dugué et al., 2015; Fiebelkorn et al., 2013; Henry et al., 2016; Landau & Fries, 2012; VanRullen et al., 2011; Zion Golumbic et al., 2013). It has been shown that slow oscillations not only govern the sampling of external input, but also control the timing of faster oscillations through phase-amplitude coupling (Canolty et al., 2010; van der Meij et al., 2012; Sauseng et al., 2019). However, it remains largely unclear how these cross-frequency interactions shape sensory processing and subsequent behavior. Here, we will investigate how the phase of slow rhythms, as well as coupling between slow and faster rhythms, correlates with behavior.

One prominent view on the alpha rhythm is that it reflects a mechanism of functional inhibition (Klimesch et al., 2007), such that increased alpha power suppresses processing in task-irrelevant regions and networks (i.e., increased alpha reflects reduced neural excitability), while decreased alpha facilitates processing in task-relevant ones (i.e., decreased alpha reflects enhanced neural excitability), effectively gating the information flow (Jensen and Mazaheri, 2010). In line with this view, it has been demonstrated that working-memory performance correlates positively with alpha activity in task-irrelevant (Haegens et al., 2010; Yu et al., 2017) and negatively in task-relevant regions (Jiang et al., 2015; van Ede et al., 2017), respectively. However, it remains unclear how this proposed alpha gating mechanism modulates the internal sensory representations (as indexed by decoding performance), with different studies reporting positive (i.e., decoding performance increases as alpha power increases; Kayser et al., 2016), negative (Barne et al., 2020), and null relationships (Griffiths et al., 2019). Here we will examine

how alpha power correlates with working-memory performance as well as the decodability of task features.

While the beta rhythm was traditionally regarded as a somatomotor rhythm (Pfurtscheller and Silva, 1999), recent evidence suggests that beta is more widely involved in top-down processing (Buschman and Miller, 2007) and long-range communication (Engel and Fries, 2010). However, the mapping between beta oscillations and low-level mechanisms is less clear-cut. One proposal is that beta oscillations play an alpha-like role, i.e., gating information processing through inhibition (Lundqvist et al., 2016; Miller et al., 2018). A more recent proposal is that beta oscillations play a facilitating role in the endogenous (re)activation of cortical content representations, e.g., during working memory and decision-making (Spitzer & Haegens, 2017). In this framework, beta-band synchronization supports the endogenous transition from latent to active cortical representations during working memory, thereby providing a readout of the information held in working memory. This proposal builds primarily upon evidence from non-human primate research (Bahmani et al., 2018; Haegens et al., 2017; Salazar et al., 2012) and is yet to be explicitly tested in the human brain (Herding et al., 2016). Here we will test the involvement of beta oscillations in circuit (re)activation, the possibility of the existence of multiple beta(s), and how these tentative different betas correlate with behavior.

Combined, we propose a comprehensive framework of oscillatory building blocks, in which slow (delta to theta) rhythms sample task-relevant input, while the alpha rhythm suppresses irrelevant input. Crucially, the beta rhythm recruits task-relevant circuits that maintain information in working memory. Finally, the timing of faster oscillations is controlled by slower rhythms via phase-amplitude coupling. Critically, we propose that oscillations (separately and combined) orchestrate the functional architecture of information processing and thereby shape behavior. In order to study this comprehensive framework, we recorded MEG in healthy participants preforming a visual delayed match-to-sample working-memory paradigm with pre- and retro-cueing.

2   Materials & Methods

2.1   Participants

Participants were 33 healthy right-handed adults (21 female, 12 male; mean age 24.6 years; range 20–33) without neurological or psychiatric disorders, who reported normal hearing and normal or corrected-to-normal vision. The study was approved by the local ethics committee (CMO 2014/288 "Imaging Human Cognition") and in accordance with the Declaration of Helsinki. Participants gave written informed consent and were remunerated for their participation.

2.2   Visual working-memory task

We used a single-item delayed match-to-sample working-memory task where participants were instructed to compare sample and probe stimuli and indicate whether the cued feature was the same or different between them (Figure 1). Each trial contained four main events: a visual cue followed by a visual sample, a second visual cue, and a probe. All events were presented at a fixed stimulus onset asynchrony (SOA) of 1.5 s. The inter-trial interval (ITI) duration was jittered between 2 and 2.4 s.

We used a two (relevant feature: orientation vs. frequency) by two (informative cue: pre- vs. retro-cue) factorial design. Participants were cued to compare sample and probe orientation in half of the trials, and spatial frequency in the other half. They were informed about the relevant feature by an informative cue, which occurred either before (pre; 50%) or after (retro; 50%) the sample presentation. These four trial types were randomly interleaved such that within each block participants performed all task conditions. Participants gave their response ("same" or "different") by pressing a button with their right index or middle finger. The response-button mapping changed on a block-by-block basis in order to avoid motor preparation confounds in our decision-related analyses.

Participants first performed a few short practice sequences of the task (20 trials each) in which feedback was provided on a trial-by-trial basis, with green and red fixation dots for correct and incorrect responses, respectively. During the main experiment, we recorded MEG while participants performed 8 blocks of 64 trials each, in which feedback was provided on a block-by-block basis. The full recording session lasted around 90 minutes.
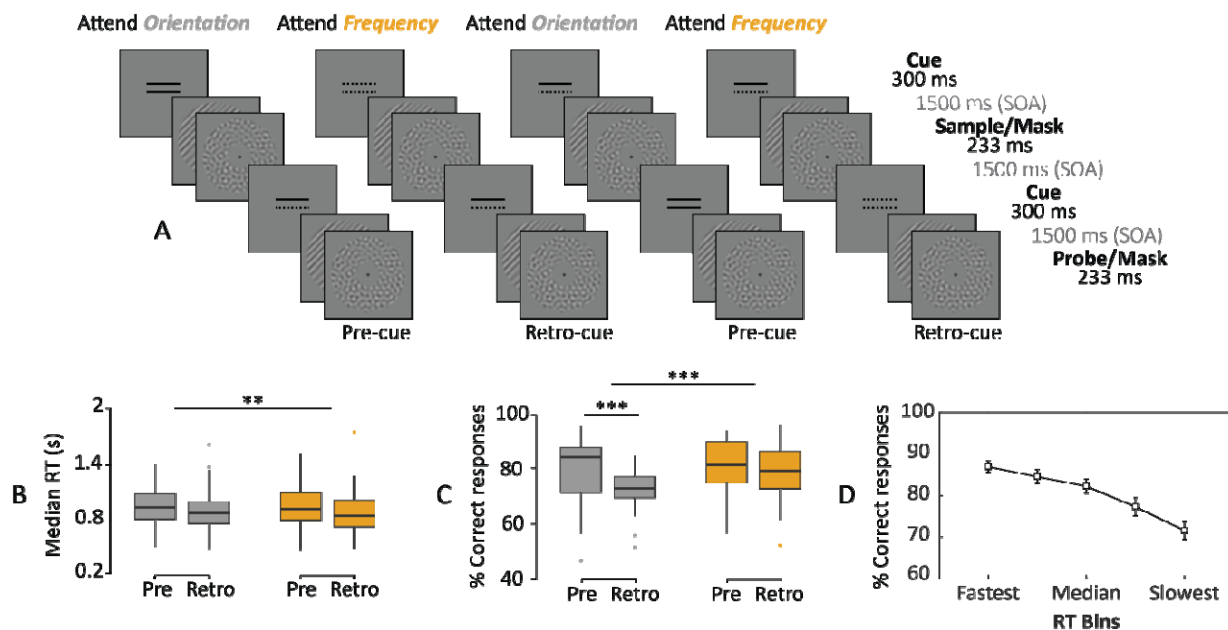
Figure 1. Paradigm and behavioral results.
[A] Schematic of the four trial types: attend orientation (two solid lines) or attend frequency (two dotted lines) for pre- and retro-cue conditions (first vs. second cue is informative; uninformative cues consist of a solid and dotted line). [B] Participants were slower and [C] more accurate matching the spatial frequency (gray bars) of the visual gratings compared to orientation (orange). This effect was mainly driven by the pre-cue condition. Within each boxplot, the horizontal line represents the median, the box delineates the area between the first and third quartiles (interquartile range). [D] Average accuracy across RT bins. Error bars represent standard error of the mean. ** $P < 0.01$, *** $P < 0.001$.

2.3 Stimuli

A bull's eye (outer black ring = 0.5° × 0.5° degree of visual angle (dva), innermost black dot = 0.25° × 0.25° dva) was presented at the center of the screen as the fixation point. Participants were instructed to always maintain fixation, and not to blink during the presentation of the stimuli. Each trial started with a cue presented for 300 ms. Next, a sample consisting of an oriented grating (Michelson contrast: 40%, spatial frequency: 1 cycle per °, orientation: 45° clockwise or counterclockwise relative to vertical, randomized spatial phase) and a backward mask (a bandpass-filtered noise patch with matched contrast and spatial frequency as the grating) were presented sequentially for 230 ms. Both the grating and the mask were shown in an annulus (inner radius = 1.5°, outer radius = 7.5°, contrast of the stimuli decreased linearly to 0 over the outer and inner 0.5° radius of the annulus) around the central fixation (Figure 1A). After an SOA of 1.5 s, a second cue was presented for 300 ms. The trial presentation finished with the probe presentation, which, similar to the sample, consisted of an oriented grating and a backward mask. The probe's cued feature matched with that of the sample grating in 50% of the trials. The experiment was programmed with PsychtoolBox (Brainard, 1997) in Matlab (Mathworks, Inc.).

2.4   Data acquisition

Stimuli were displayed on a semitranslucent screen (1920 × 1080-pixel resolution, 120-Hz refresh rate) back-projected by a PROpixx projector (VPixx Technologies) during MEG recordings. Whole-head MEG data were acquired at a sampling frequency of 1200 Hz with a 275-channel MEG system with axial gradiometers (CTF MEG Systems, VSM MedTech Ltd.) in a magnetically shielded room. Six permanently faulty channels were disabled during the recordings, leaving 269 recorded MEG channels. Three fiducial coils were placed at the participant's nasion and both ear canals, to provide online monitoring of participant's head position (Stolk et al., 2012) and offline anatomical landmarks for co-registration. Eye position was recorded using an eye tracker (EyeLink, SR Research Ltd.). Upon completion of the MEG session, participant's head shape and the location of the three fiducial coils were digitized using a Polhemus 3D tracking device (Polhemus, Colchester, Vermont, United States). Anatomical T1-weighted MRIs were obtained during a separate session. To improve co-registration of the MRIs and MEG data, earplugs with a drop of Vitamin E were placed at participant's ear canals during MRI acquisition. These anatomical scans were used for source reconstruction of the MEG signals.

2.5   Behavioral analysis

The influence of cue condition (two levels: pre- and retro-cue) and feature (two levels: orientation and spatial frequency) on median reaction time (RT; including correct responses only) and accuracy (percentage of correct responses) was tested using a linear mixed-effects model using the lme4 package (Bates et al., 2015) for R (Team, 2013). For post-hoc analysis we used the Lsmean package (Searle et al., 1980) where p-values were considered as significant at p<0.05 and adjusted for the number of comparisons performed (Tukey method).

2.6   MEG pre-processing

MEG data were preprocessed offline and analyzed using the FieldTrip toolbox (Oostenveld et al., 2010) and custom-built MATLAB scripts. The MEG signal was epoched based on the onset of the first cue (t= -1 to 7s). The data were downsampled to a sampling frequency of 300 Hz, after applying a notch filter to remove line noise and harmonics (50, 100, and 150 Hz). Bad channels and trials were rejected via visual inspection before independent component analysis (Jung et al., 2001) was applied. Subsequently, components representing eye-related and heart-related artefacts were projected out of the data (on average, four components were removed per participant). Finally, outlier trials of extreme variance were removed. This resulted in an average of 393 (± 9 SEM) trials and 268 channels per participant for the reported analyses.

2.7   Event-related fields

Single-trial data were baseline corrected (t = –0.1 to 0 s) before calculation of first-cue and grating locked event-related fields (ERFs). In addition, a planar representation of the MEG field distribution was calculated from the averaged data (ERFs) using the nearest-neighbor method. This transformation makes interpretation of the sensor level data easier as the signal amplitude is typically maximal above a source.

2.8   Spectral analysis

Our analysis aimed to highlight the (1) differential impacts of pre- and retro-cueing on the oscillatory dynamics of interest, and (2) the behavioral relevance of these dynamics. For the cueing contrast, spectral measures were compared between pre- and retro-cue trials (including correct response trials only). For the behavioral contrast, trials from all conditions (including both correct and incorrect response trials) were pooled together and divided into five quantile bins (approx. 80 trials per bin) according to RT. Spectral measures were contrasted between the slowest and fastest RT bins, to maximize statistical power.

For the 20 MEG channels displaying the maximal post-grating ERFs (channels selected individually per participant), we extracted 1-s pre-stimulus windows (t = –1 to 0 s), multiplied these with a Hanning taper, and computed power spectra (1–30 Hz; 1-Hz resolution) using a fast Fourier transform (FFT) approach. In order to determine the individual alpha peak frequency, we detected the highest local maximum within the 7–14 Hz band. In order to detect the beta peak frequency, linear regression (least-squares fit) was used to fit a linear model to the log-transformed spectrum in the beta range in order to compensate for the 1/f effect. The fitted linear trend was then subtracted from the spectrum, allowing for a more reliable beta peak frequency estimate within the 15–30 Hz band (Haegens et al., 2014).
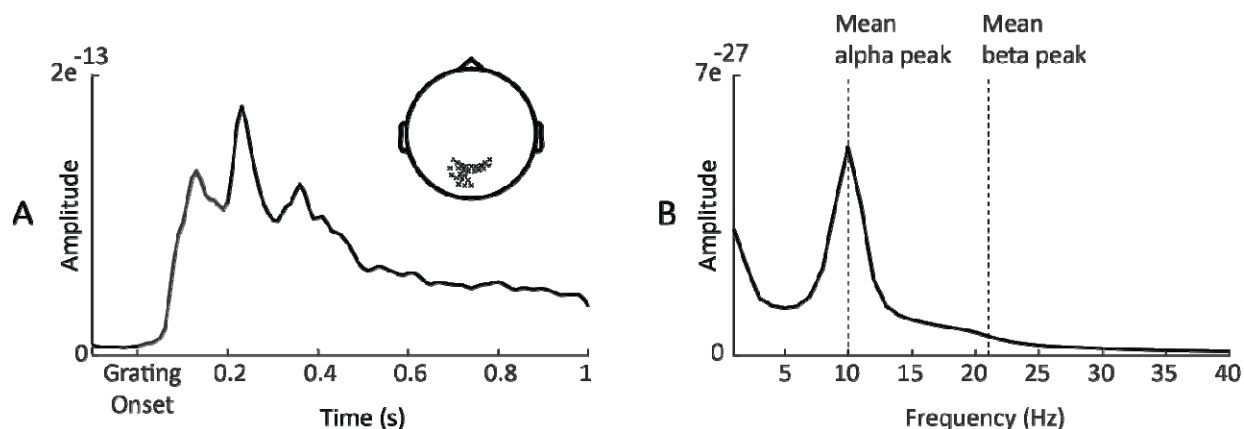

Figure 2. Alpha and beta peak detection.
[A] Grand-averaged ERF of sensors (highlighted in sensor space) displaying maximal post-grating ERFs within 200 ms following the grating onset. Gray shaded area around the curve denotes between-participants standard error. Light gray shaded box highlights the time period used to select channels with maximal post-grating ERFs. [B] Power spectra (averaged over same sensors marked in A; t = -1 to 0 s relative to first cue onset) showing alpha and beta peaks.

We identified distinct alpha peak frequencies for all participants (mean = 9.9 Hz ± 0.21 SEM; Figure 2), while for beta we identified peaks for 18 participants (mean = 20.8 Hz ± 0.37 SEM) and assigned the mean beta peak for the remainder of the participants (N=15). In order to create peak-centered signals, we computed TFRs of the power spectra for the full trials per experimental condition. To this end, we used an adaptive sliding time window of five cycles

length per frequency (Δt = 5/f; 20-ms step size), and estimated power after applying a Hanning taper. We created theta-peak (4 Hz), alpha-peak (individualized) and beta-peak (individualized) centered time-resolved signals with spectral bandwidths of 2 Hz, 2 Hz and 4 Hz, respectively. Power normalization was performed relative to a baseline (t = -0.4 to -0.2 s) for the cueing contrast and relative to the average of all RT bins for the RT contrast.

We estimated intertrial phase coherence (Tallon-Baudry et al., 1996) across trials, for each time point, frequency and sensor, for each RT bin separately. This measure reflects the degree to which the phase of each frequency is aligned across trials. In addition, we used the Tensorpac toolbox (Combrisson et al., 2020) to compute a time-resolved measure of phase-amplitude coupling (PAC) on source level. This algorithm measures PAC across trials (rather than across time).

2.9   Statistical analysis

In order to investigate whether differences between conditions of interest (cueing contrast: pre- vs. retro-cue; RT contrast: slowest vs. fastest RT bin) were statistically significant, we used nonparametric cluster-based permutation analysis (Maris and Oostenveld, 2007). In brief, this test first calculates paired t-tests for each sensor at each time and/or frequency point, which are then thresholded at $p < 0.05$ and clustered on the basis of temporal, spatial and/or spectral adjacency. The sum of t-values within each cluster is retained, and the procedure is repeated 1000 times on permuted data in which the condition assignment within each individual is randomized. On each permutation, the maximum sum is retained. Across all permutations, this yields a distribution of 1000 maximum cluster values. From this distribution, the probability of each empirically observed cluster statistic can be derived (evaluated at alpha = 0.05).

2.10   Source reconstruction

For each participant, an anatomically realistic single-shell headmodel based on individual T1-weighted anatomical images was generated (Nolte, 2003). A grid with 0.5-cm resolution was created using an MNI template onto which the brain volume of each participant was morphed using non-linear transformation. For each grid point, leadfields were computed with a reduced rank, which removes the sensitivity to the direction perpendicular to the surface of the volume conduction model. This procedure ensures that each grid point represents the same anatomical location across all participants.

In order to visualize the sources of our sensor-level spectrotemporal (power and ITC) and temporal effects (ERFs), we utilized the frequency-domain adaptive spatial technique of dynamical imaging of coherent sources (DICS; Gross et al., 2001) and the linearly constrained minimum variance beamformer (LCMV; Van Veen et al., 1997), respectively. Data from all conditions of interest were concatenated in order to compute the cross-spectral density (CSD) matrices (t= -1 to 2 s; multitaper method (Mitra & Pesaran, 1999)) and the covariance matrices of the averaged single trials (t= -0.6 to 5.5 s; lambda 5%) for the DICS and LCMV beamformer, respectively. Leadfields for all grid points along with the CSD/covariance matrices were used to compute a common spatial filter (i.e., common for all trials and conditions) that was used to

estimate the spatial distribution of power/amplitude for our windows of interest. The source orientation was fixed to the dipole orientation with the highest strength.

Finally, the PAC analysis was performed on source level (i.e., virtual channels), for which the source space was subdivided into 22 anatomically defined brain parcels (Wallis et al., 2015). Sensor-level time-series data were multiplied by spatial filters (constructed using LCMV beamformer) in order to obtain the time-resolved activity in each virtual channel.

2.11 Multivariate pattern analysis

To investigate how oscillatory dynamics influence the information content of neural activity, we were interested in decoding two task features: (1) informative cue instruction (attend orientation or spatial frequency), and (2) sample (i.e., the first grating) properties (orientation: clockwise or counterclockwise; spatial frequency: low or high). For all multivariate pattern analysis (MVPA), we used MNE Python (Gramfort et al., 2013) and Scikit-learn (Pedregosa et al., 2012). We implemented a 4-fold cross-validation procedure within each participant. For each timepoint, we trained a logistic regression classifier (L2-regularized) on three folds and tested on the left-out fold. The analysis was shifted over time on a sample-by-sample basis. The input signal was the broadband signal lowpass filtered at 35 Hz (Gwilliams & King, 2020; King et al., 2016). We operationalized the decoding accuracy as area under the curve (AUC) by evaluating the similarity between the true label categories of the test set and the probabilistic class labels (normalized distance from the fit hyperplane: "predict_proba" in scikit-learn) of the same trials. We computed the AUC under the null hypothesis by randomly shuffling the label categories and obtained a p-value as the proportion of the null AUC estimates that exceeded the true AUC (evaluated at alpha = 0.05).

We aimed to first demonstrate the decodability of the aforementioned features from the broadband time-domain signal. We used trials from all conditions and tested decoding accuracy against chance level (i.e., AUC = 0.5 for binary classification) using nonparametric cluster-based permutation analysis (as described above). All task features could be decoded from the MEG signal: informative cue instruction (attend to frequency or orientation), grating orientation (clockwise or counterclockwise) and spatial frequency (low or high). For cue identity, group-level decoding performance peaked around 150 ms after the onset of the first/second cue for the pre-/retro-cue conditions, respectively (Figure 3AB), while for grating properties, group-level decoding performance (for orientation and spatial frequency) peaked around 100 ms (Figure 3CD).
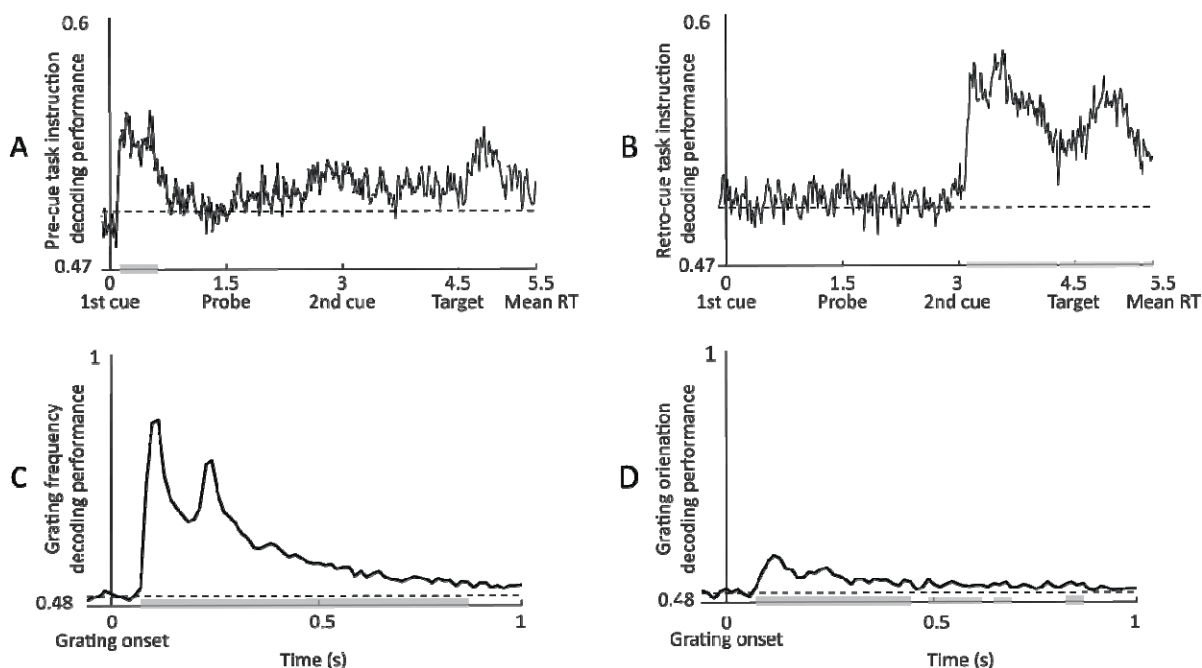
Figure 3. Decodability of task features.
[A] Temporal sample-by-sample decoding of cue features (attend frequency vs. attend orientation) for pre- and [B] retro-cues. [C] Decoding performance for grating spatial frequency (low vs. high) and [D] grating orientation (clockwise vs. counterclockwise). Gray bars indicate significance of decoding accuracy (t-test vs. chance).

Next, we asked whether oscillatory state shapes neural stimulus representations as reflected by decoding performance. To test this, we evaluated how decoder accuracy was related to trial-by-trial fluctuations of prestimulus power. We used the classification procedure explained above, replacing the k-fold cross validation with a leave-one-out cross-validation (LOOCV) procedure. In LOOCV, the classifier is fit to all trials but one, evaluating model performance on the remaining "left-out" trial as a single-item test set. This is advantageous because: (1) it allows a maximal amount of data to be used for training, thus reducing noise in the model fit; (2) it provides an unbiased single-trial decoding estimate, which can be analyzed by a binning approach. For each timepoint and test trial, we computed the probabilistic estimates of the logistic regression for our feature of interest (cue information) and then grouped these results into five bins relative to occipital sensor theta, alpha and beta power. Afterwards, for each frequency band separately, the time-resolved AUC signal was contrasted between the bins of lowest and highest power using nonparametric cluster-based permutation analysis.

Finally, to investigate the evolution of sample representations, we utilized the temporal generalization method (King & Dehaene, 2014). For this analysis, each classifier was trained on time T and tested on its ability to predict a given trial at time T'. This method estimates the similarity of the coding pattern at T and T', and thus the stability of the neural representation. In order to facilitate the interpretation of our results, we averaged the AUC for training times within the first 0.3 s following the sample onset. This was done separately for each bin and each

band, followed by contrasting the averaged temporal generalization matrices between the bins of lowest and highest power using nonparametric cluster-based permutation analysis.

2.12 Data and code availability

All data and code used for stimulus presentation and analysis are available online at the Donders Repository at https://doi.org/10.34973/tqy5-mh37.

3   Results

3.1   Behavioral results

In order to test our framework, we recorded MEG data from 33 healthy participants who performed a delayed match-to-sample working-memory paradigm where they evaluated orientation or spatial frequency of two visual gratings. The to-be-matched feature was indicated by a visual cue occurring either before (pre-cue) or after (retro-cue) sample presentation.

Overall, participants were faster matching the orientation than the spatial frequency of the gratings ($F(1,32) = 11.2$, $p = 0.001$; Figure 1B). There was no significant difference in RT between cue conditions ($F(1,32) = 2.7$, $p = 0.07$), nor a significant interaction between feature and cue conditions ($F(1,128) = 12.7$, $p = 0.66$). In terms of accuracy, participants were better at matching spatial frequency than orientation ($F(1,128) = 13.4$, $p < 0.001$; Figure 1C). There was no significant difference in accuracy between cue conditions ($F(1,128) = 2.7$, $p = 0.10$), though there was a significant interaction between the cue and feature conditions ($F(1,128) = 12.7$, $p < 0.001$): when matching the orientation of gratings, participants were better in the pre-cue than the retro-cue condition ($t(32) = -3.7$, $p < 0.001$), whereas when matching the spatial frequency of gratings, participants performed similarly in both cue conditions ($t(32) = 1.35$, $p = 0.17$).

Note that the absence of main cue effects demonstrates that task difficulty (performance) was comparable across our conditions of interest (i.e., pre- and retro-cue) and therefore does not constitute a confound in our subsequent analyses. Furthermore, accuracy linearly decreased with increasing RT ($R^2 = 0.21$, $p < 0.001$; Figure 1D), suggesting no speed-accuracy tradeoff.

3.2   Impact of cueing on oscillatory dynamics

In order to establish the proposed low-level mechanisms, we first investigated the differential impacts of pre- and retro-cueing on oscillatory power for the respective bands of interest. The critical difference between the pre- and retro-cue conditions is the time when participants are informed about the task-(ir)relevant feature. If alpha/beta decrease is critical for the inhibition of task-irrelevant features, we expect alpha/beta power decrease to be contingent upon the informative cues, after which selection (i.e., inhibition of the task-irrelevant feature and/or enhancement of the relevant one) is possible.

Indeed, we found significant differences between pre- and retro-cue conditions for all our frequency bands of interest (Figure 4A). Following the first cue, alpha and beta power decrease was stronger for the pre-cue condition (in which the first cue was informative) in comparison to the retro-cue condition (Figure 4CD; cluster-based permutation test, $p = 0.002$ and 0.003; $t = 0.35$ to 1 s and 0.34 to 0.77 s; centered on occipitoparietal and temporal sensors). Differences between pre- and retro-cue conditions were mainly localized to left and right occipital cortices, and right middle and superior temporal gyri.

This pattern was reversed following the second cue, with alpha and beta power decrease being stronger for the retro-cue condition (in which the second cue was informative) in comparison to

the pre-cue condition (Figure 4CD; p = 0.001; t = 3 to 4 s and 2.6 to 3.6 s; centered on occipitoparietal sensors). In addition, beta power decrease was stronger for the pre-cue vs. retro-cue condition just prior to the probe presentation (Figure 4D; p = 0.004; t = 3.8 to 4.4 s; centered on occipital sensors). Differences between pre- and retro-cue conditions were mainly localized to left and right occipital cortices and the precentral gyrus, with beta effects extending more towards the dorsolateral prefrontal cortex.

Furthermore, following the second cue, theta power decrease was stronger for the pre-cue condition in comparison to the retro-cue condition (Figure 4B; p = 0.02; t = 3.7 to 4.7 s; centered on occipital sensors). Differences between pre- and retro-cue conditions were mainly localized to right occipital cortices and right temporoparietal junction.

To summarize, the informative cue (i.e., the first cue on pre-cue trials and the second cue on retro-cue trials) was followed by a stronger decrease in alpha and beta power, consistent with the functional inhibition account. In addition, the informative cue on retro-cue trials was followed by a weaker decrease in theta power. While we did not expect this theta effect, we posit that it reflects enhanced processing of the informative cue as it has been proposed that theta power provides optimal neural "ambiance" for information processing (Colgin, 2012; Klimesch, 1999; Sauseng et al., 2010), which is in line with theta's role in our framework: regulating input sampling.
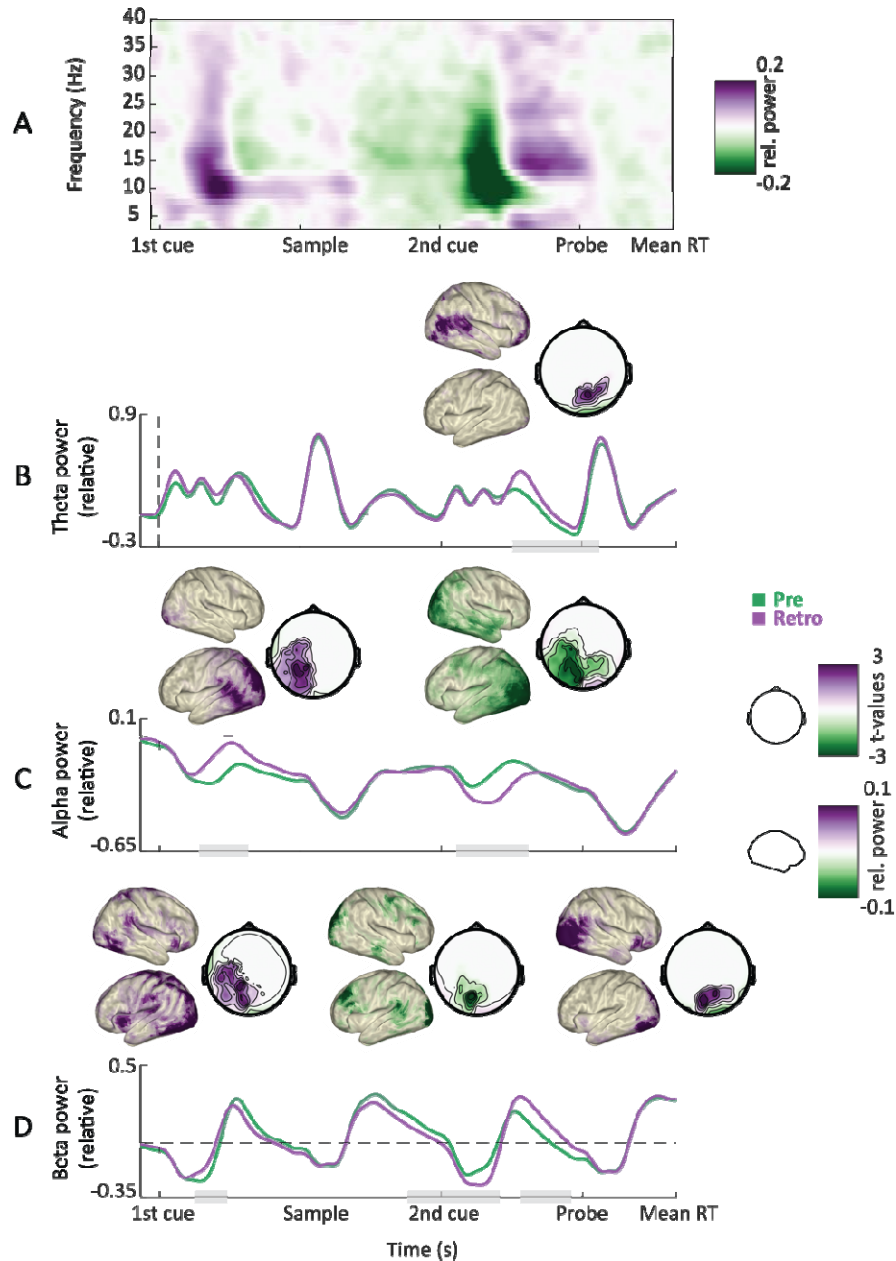
Figure 4. Cue-related power modulations.
[A] Time frequency representations (TFRs) highlighting the relative change in power between the pre- and retro-cue conditions. [B] Time course of oscillatory activity averaged within the theta band for the pre- (green) and retro-cue conditions (purple). Shaded areas denote between-participants standard error. Gray bars on the x-axis indicate significant differences between conditions. Topographies show statistical and power distributions of these significant differences in sensor and source space, respectively. [C] Same as B for alpha and [D] beta bands.

3.3 Impact of oscillatory dynamics on behavioral performance

Next, we asked whether any of the observed oscillatory dynamics impacted behavioral performance. We expected that faster responses would coincide with (1) an increase in the phase alignment of slow rhythms, reflecting their role in input sampling and temporal prediction, (2) a decrease in occipital alpha/beta power, reflecting their gating role, and (3) increased phase-amplitude coupling between slow and fast rhythms, reflecting the temporal coordination of fast rhythms by slower ones. We binned trials into five bins based on RT and contrasted oscillatory dynamics between bins of the slowest and fastest RT to test these predictions.

In line with our predictions, faster responses were associated with weaker alpha and beta power before and during probe presentation (Figure 5BC; p = 0.002 and 0.001; t = 4.1 to 5.1 s; centered on occipitoparietal sensors). These effects were localized to occipital cortices and the left inferior and parietal cortices. Furthermore, faster responses were associated with stronger theta power before probe presentation (Figure 5A; p = 0.001; t = 2.3 to 4.1 s; centered on temporal and frontal sensors). These effects localized to prefrontal and frontal cortices.
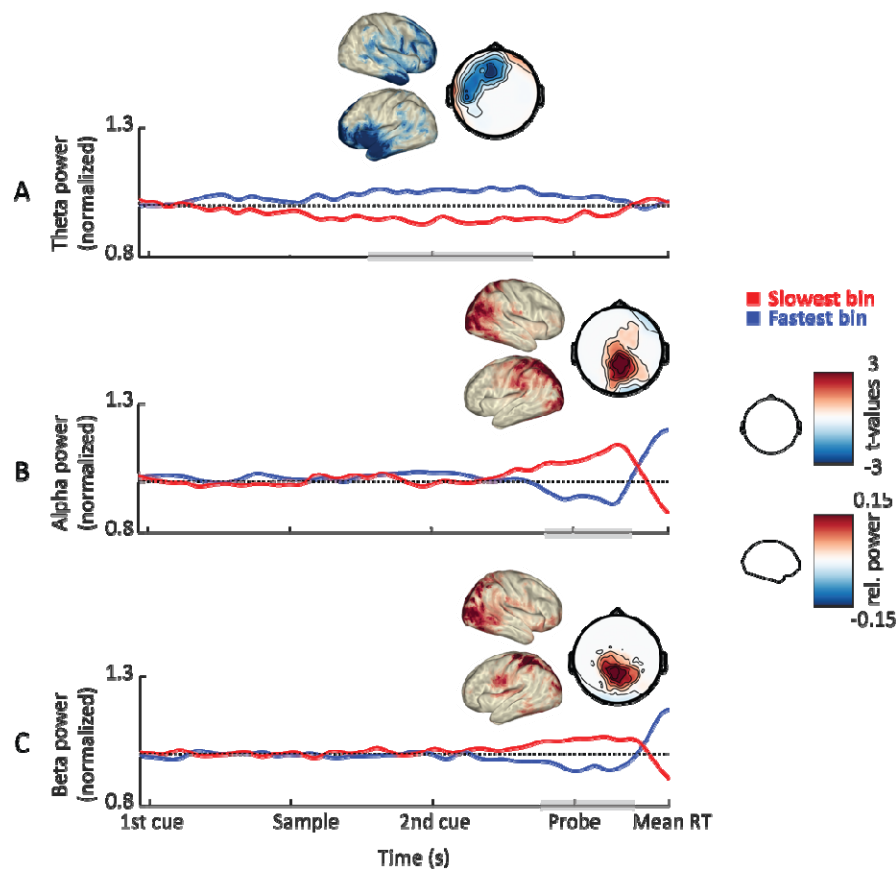

Figure 5. Correlates of behavioral performance: Power.

[A] Time courses of the normalized oscillatory activity averaged within the theta band for the slowest (red) and fastest RT bin (blue). Shaded areas denote between-participants standard error. Gray bars indicate significant differences between conditions. Dashed lines represent mean power (i.e., normalized power = 1). Topographies show statistical and power distributions of these significant differences in sensor and source space, respectively. [B] Same as A for alpha and [C] beta bands.

In addition to these power effects, faster responses were accompanied by an increase in ITC in lower frequencies (Figure 6AB; p < 0.001; t = 4.4 to 5.5 s; f = 1 to 5 Hz; widespread sensors). Differences were maximal in left and right post- and precentral gyri and lateral prefrontal cortices. We found that the coupling between the phase of 1–3 Hz oscillations and the amplitude of 30–35 Hz oscillations was stronger for fast vs. slow RT in the intraparietal sulcus (Figure 6C; p = 0.02; t = 0 to 5.5 s) and the superior parietal lobe (Figure 6D; p = 0.07; t = 0 to 3 s). Combined, these results indicate that response speed was influenced by the phase alignment of delta-to-theta oscillations as well as phase-amplitude coupling between slow and fast rhythms.
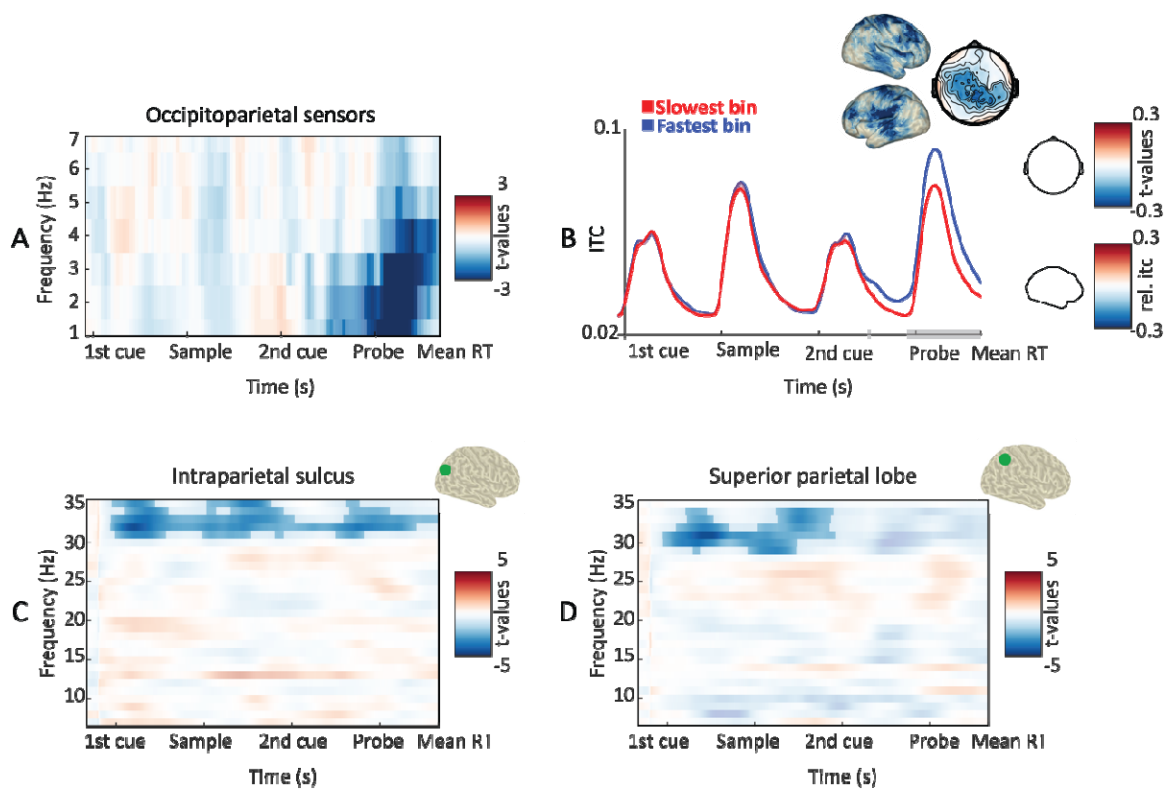

Figure 6. Correlates of behavioral performance: ITC and PAC.
[A] TFR of statistical differences in ITC between the slowest and fastest RT bins (masked at p < 0.05). [B] Averaged ITC time course (1–5 Hz) for slowest (red) and fastest RT bins (blue). Shaded areas denote between-participants standard error. Gray bars indicate significant differences between conditions. Topographies show statistical and power distributions of these significant differences in sensor and source space, respectively. [C] TFR of statistical differences in PAC between the slowest and fastest RT bins (masked at p < 0.05) in the intraparietal sulcus (as highlighted in green on brain surface). Negative values (blue) indicate higher PAC for the fastest RT bin. [D] Same as C for the superior parietal lobe.

To ensure that the ITC results did not stem from low-frequency evoked (phase-locked) responses, we ran two additional (control) analyses. First, we performed the abovementioned ITC analyses after subtraction of the evoked response from single-trial data. The results were similar to those of our previous analysis, i.e., faster responses were accompanied by an increase in ITC (p < 0.001; t = 4.7 to 5.4 s; f = 1 to 4 Hz; widespread), indicating that the low-frequency modulations cannot be fully explained by evoked activity. In addition, we compared ERFs between RT bins, and found that ERF amplitude was higher for the fastest compared to the slowest RT bin (Figure 7; p < 0.05; t = 3.7 to 5.5 s; centered on occipitoparietal sensors). Differences were widespread but maximal in the right occipital cortex, right inferior parietal and supramarginal gyri. It is important to note that the localization of the ERF effects is not identical to that of the ITC effects, which were maximal in more anterior regions, suggesting that these effects (ERF and ITC) might reflect two separate phenomena.
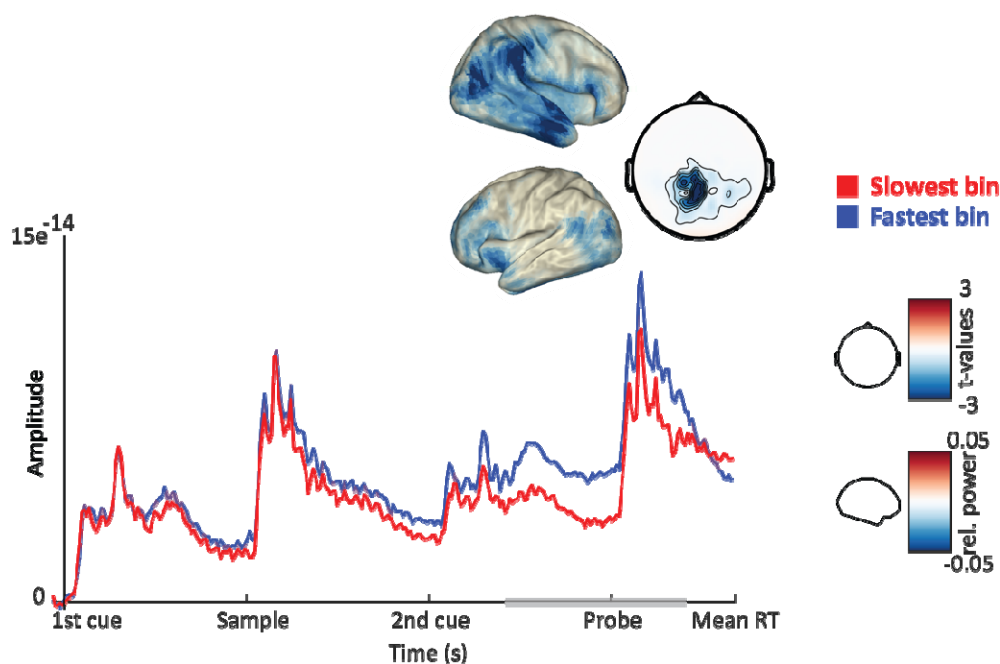

Figure 7. Correlates of behavioral performance: ERFs.
Grand average ERFs (occipital sensors) for the slowest (red) and fastest bins (blue). Shaded areas denote between-participants standard error. Gray bars indicate significant differences between conditions. Topographies show statistical and power distributions of these significant differences in sensor and source space, respectively.

In sum, faster RT was preceded by (1) an increase in phase alignment and power of slow oscillations, consistent with a role in regulating input sampling, (2) a prominent occipitoparietal alpha/beta decrease, consistent with a gating-through-inhibition mechanism, and (3) an increased phase-amplitude coupling between slow and fast oscillations, consistent with a role of slow oscillations in temporal control of faster oscillations.

3.4   Impact of oscillatory dynamics on decoding performance

Finally, we investigated how oscillatory dynamics influence the information content of neural activity patterns. We expected this content, indexed by classification accuracy, to be boosted by a decrease in alpha power (i.e., release of inhibition) and an increase in beta power (reflecting circuit recruitment). We trained neural classifiers to decode two task features: (1) informative cue instruction (attend orientation or spatial frequency), and (2) grating properties (orientation: clockwise or counterclockwise; spatial frequency: low or high).

Using a LOOCV procedure, we obtained unbiased single-trial responses of the classifiers. We then grouped these single-trial estimates into five bins relative to occipital theta, alpha and beta power, and contrasted the decoding accuracy between bins of the lowest and highest pre-cue power. In accordance with our alpha predictions, we found significant differences contrasting decoding accuracy between bins of low and high pre-stimulus occipital alpha power for pre-cue instruction (Figure 8A; p = 0.024; t = 0.2 to 0.21 and 0.47 to 0.49 s). In other words, decoding accuracy was higher for cues that were preceded by low alpha power. No significant effects were found for the decodability of retro-cue instruction by alpha power (p = 0.37).

In accordance with our beta predictions, we found significant differences contrasting decoding accuracy between bins of low and high beta power for pre-cue instruction (Figure 8B; p = 0.048; t = 0.26 to 0.27 s). In addition, we found a trend contrasting decoding accuracy between bins of low and high beta power for retro-cue instruction (p = 0.057; t = 0.37 to 0.39 s). Thus, contrary to alpha power, decoding accuracy was higher for cues that were preceded by high beta power. No significant modulations were found for the decodability of pre- or retro-cue instruction by theta power (p > 0.5 and p = 0.21, respectively), suggesting that this modulation of neural stimulus information was specific to alpha and beta oscillations.
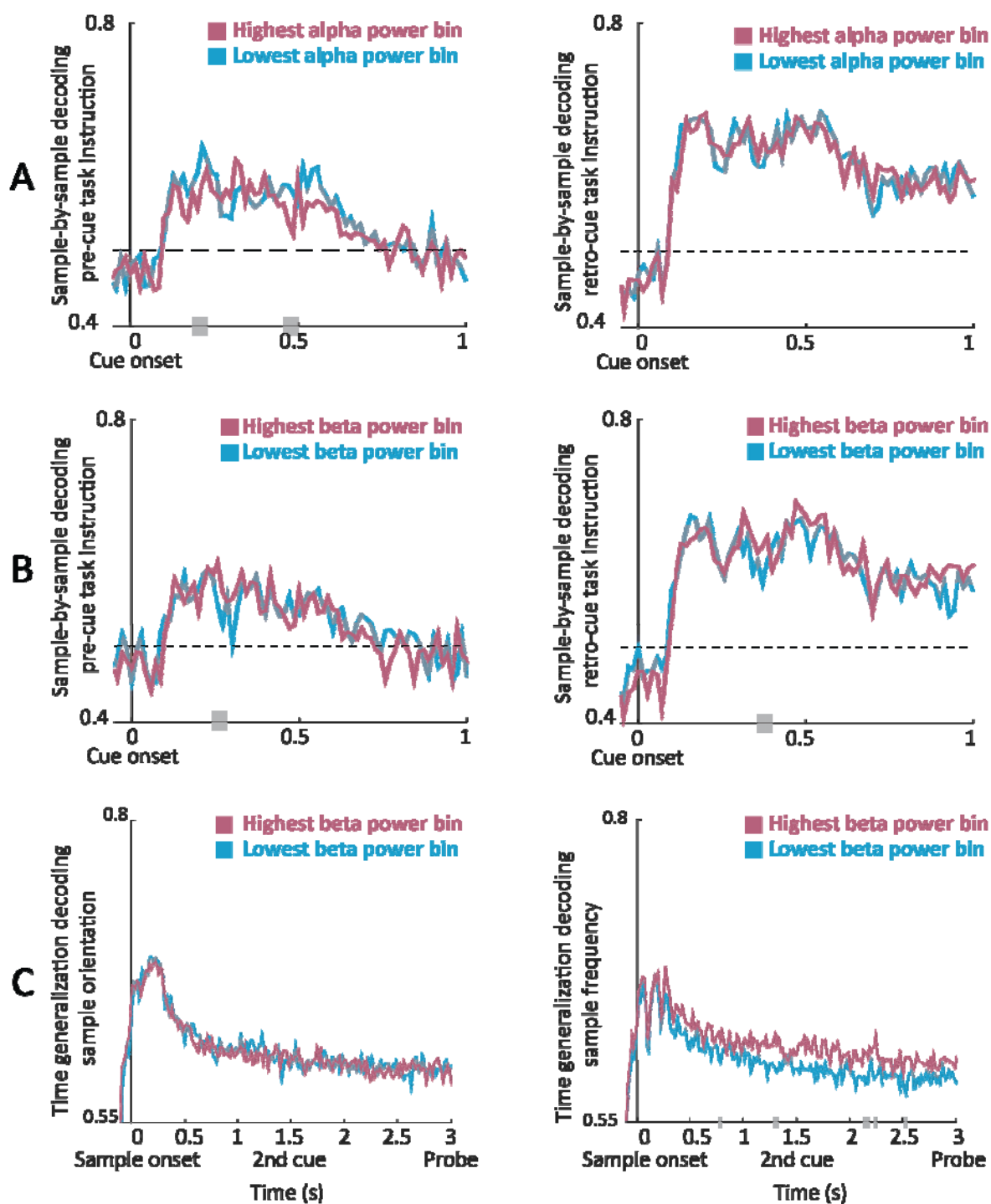
Figure 8. Effects of pre-stimulus oscillatory power on decodability.
[A] Temporal sample-by-sample decoding of pre-cue (left panel) and retro-cue (right panel) instruction for the bins of lowest and highest occipital alpha power preceding cue onset. [B] Same as A for the beta band. [C] Averaged time-generalization matrices (over the first 0.3 s of training time) of decoding the sample's orientation (left panel) and frequency (right panel) for the bins of lowest and highest beta power preceding sample onset. Gray bars indicate significant differences between low and high power bins.

In order to further test our predictions regarding beta power and (reactivation of) information content, we focused on decoding the spatial frequency and orientation of the sample stimulus. To this end, we applied a time-generalization approach in which the classifier was trained at each time point and tested on all other time points, thus allowing us to test the temporal stability of the information content. This approach yields a two-dimensional matrix across training and testing times. In order to reduce dimensionality, we averaged decoding accuracy across the early training time points (0 to 0.3 s post sample onset). We then contrasted the averaged decoding accuracy between the bins of lowest and highest pre-stimulus power.

In line with our predictions, we found significant differences between the averaged time-generalization matrices for decoding spatial frequency of the sample stimulus between bins of low and high occipital beta power (Figure 8C; p = 0.022). In other words, in trials where the sample was preceded by high beta power, classifiers trained on early time points more accurately decoded the sample's spatial frequency when tested on later time points (0.8 to 2.5 s) in comparison to trials preceded by low beta power. No significant effects were found for the decodability of the sample's orientation (p = 0.47) based on beta binning, though note that overall decoding performance was much lower for orientation than frequency (compare Figure 3 panels C and D for overall decoding performance along the diagonal).

No significant effects were found for the decodability of the sample's spatial frequency or orientation when binning was performed according to theta (p = 0.11 and p = 0.2, respectively) or alpha power (p = 0.38, p = 0.46), suggesting that the maintenance of neural stimulus information was specifically supported by beta oscillations.

In summary, alpha and beta oscillations differentially modulated the information content of neural activity. We found a negative relationship between alpha power and cue representations, as predicted by the inhibitory gating account, while we found a positive relationship between beta power and cue and sample representations, as predicted by the circuit recruitment account.

4   Discussion

In this study, we used a delayed match-to-sample working-memory task with pre- and retro-cueing in order to study a comprehensive framework that integrates the functional roles of specific neural oscillations, and, critically, the coordination between them. We directly tested our proposed framework in which slow rhythms sample task-relevant input, while alpha/beta gates the information flow by suppressing task-irrelevant processing, and beta further serves to recruit task-relevant circuits. Crucially, via phase-amplitude coupling, the timing of faster oscillations is controlled by slower rhythms. Indeed, in line with their role as a pace keeper of input sampling, we found that successful matching of probe and sample stimuli was preceded by an increased phase alignment that was confined to slow rhythms. As for the gate keeping role of alpha oscillations, we demonstrated a pattern of alpha decrease that temporally tracked the presentation of the informative cue, correlated with faster behavioral performance and increased neural information content (indexed by decoding performance). Importantly, we shed new light on the dual role of beta oscillations: on the one hand, an alpha-like inhibitory role, gating the processing of relevant input, and on the other hand, a circuit-activation role, relevant for (reactivation of) information maintenance.

4.1   Slow oscillations: the pace keeper

The first tenet of our framework is slow oscillations (1–7 Hz): we hypothesized that their phase regulates the sampling of task-relevant input and controls the timing of faster oscillations via phase-amplitude coupling. Indeed, we demonstrate that intertrial coherence (i.e., phase alignment) of slow oscillations was more prominent for trials with the fastest responses. Interestingly, this effect occurred before probe onset and was maximal in the pre- and post-central gyri and lateral prefrontal cortex. We also found that on fast trials, the phase of slow oscillations was more strongly coupled to the amplitude of faster oscillations (in the high beta range) in parietal areas.

We posit that this behavioral facilitation relies on more optimal temporal coordination reflected in the phase adjustment of slow oscillations and their coupling to faster oscillations, which in turn reflects better temporal prediction of probe onset. This is in line with previous reports that temporal predictions are associated with improved behavioral performance (Coull & Nobre, 1998; Miniussi et al., 1999; Nobre et al., 2007) and increased phase alignment of slow oscillations (Breska & Deouell, 2017), as well as recent evidence that the phase of slow oscillations predicts behavioral performance (Herbst & Obleser, 2019). This finding further corroborates previous reports of cross-frequency interactions during working memory (Bahramisharif et al., 2018; Bastos et al., 2018; Berger et al., 2019) and adds to a growing number of studies demonstrating the behavioral relevance of such coupling (Axmacher et al., 2010; Puszta et al., 2020). Thus, temporal coordination by slow oscillations governs the sampling of incoming stimuli (Busch et al., 2009; Fiebelkorn et al., 2013; Landau and Fries, 2012; VanRullen et al., 2011) and controls the timing of faster oscillations.

In addition, we found that increased theta power prior to probe onset in (pre-) frontal areas was followed by faster responses. This is consistent with previous reports showing frontal theta

enhancement during working-memory maintenance (Costers et al., 2020; Gudi-Mindermann et al., 2020; Hsieh et al., 2011; Jensen & Tesche, 2002). While we did not predict a theta power modulation, this effect is consistent with the temporal coordination role in our framework as it is proposed that theta power organizes neural assemblies into a sequential code. Thus, theta power maintains the temporal relationships between items held in working memory (Colgin, 2012; Klimesch et al., 2005; Roux & Uhlhaas, 2014).

Finally, in addition to these delta/theta dynamics, we found that faster behavioral performance cooccurred with stronger ERFs preceding and following probe onset (i.e., contingent negative variation or CNV, and N1/P2 and P3, respectively). This ERF enhancement may reflect better temporal prediction of probe onset in fast trials, resulting in a more prominent anticipatory ramping up of neural activity (Bidet-Caulet et al., 2015; Breska & Deouell, 2017; Brunia & Boxtel, 2001). One potential concern is that our spectral analysis picked up on this evoked activity (rather than genuine oscillatory dynamics). However, given that our phase results were not substantially altered by removing evoked activity and that delta/theta and ERF dynamics were not identically localized, we posit that these changes in evoked activity reflect an additional aspect of anticipatory mechanisms that are boosted by slow rhythm phase modulations, i.e., enhanced phase alignment leads to a stronger evoked response.

In summary, we provide novel insights on how slow oscillations not only coordinate input sampling but also faster oscillatory dynamics for optimal information processing and behavioral performance. Future research should investigate how this endogenous rhythmic sampling mechanism is deployed in contexts of fixed versus varying temporal structure.

4.2   Alpha oscillations: the gate keeper of information processing

We found that decreases in alpha power actively track the presentation of informative cues; i.e., regardless of its position in time, the informative cue was followed by a more prominent decrease in occipitoparietal alpha power. Our results are in line with the proposed gating role for alpha oscillations: once an input has been sampled through slow oscillations, its subsequent processing depends on its task relevance, i.e., alpha oscillations up- and down-regulate cortical excitability in task-relevant and irrelevant networks, respectively (Jensen & Mazaheri, 2010; Klimesch et al., 2007). This regulation of cortical excitability has been shown to occur spontaneously (Iemi et al., 2019; Linkenkaer-Hansen et al., 2004; Samaha et al., 2017; van Dijk et al., 2008) or to track relevant input in space (Mazaheri et al., 2014; ElShafei et al., 2018; Haegens et al., 2012,Thut et al., 2006) or, as in the case of the current study, in time (Hanslmayr et al., 2011; Rohenkohl & Nobre, 2011; van Diepen et al., 2015; van Ede et al., 2017).

In addition, we found that faster responses were preceded by more prominent occipitoparietal alpha power decrease. This is in line with previous studies demonstrating that behavioral performance correlates negatively with alpha activity in task-relevant (Jiang et al., 2015; van Ede et al., 2017) and positively in task-irrelevant regions (Haegens et al., 2010; Yu et al., 2017). Both lines of results reflect the same low-level gating mechanism deployed to allocate more resources to task-relevant networks, either by directly boosting the processing of task-relevant

information or by suppressing that of task-irrelevant information (i.e., distracting or competing stimuli).

Importantly, we demonstrate that pre-stimulus alpha power decrease enhances neural decodability (i.e., sensory representations) of subsequent task-relevant items. These results are in line with previous work reporting a negative relationship between decoding performance and pre-stimulus alpha power (Barne et al., 2020; van Ede et al., 2018), and shows how alpha through regulating cortical excitability might influence sensory representations.

4.3   Beta oscillations: a dual role in information gating and circuit formation

We hypothesized that multiple beta mechanisms exist, with one beta mechanism playing a local functionally inhibitory role ("inhibitory beta"), similar to alpha, and another beta mechanism allowing top-down flexible activation of task-relevant circuits that maintain the information required to successfully perform the task at hand ("circuit beta"). These two mechanisms translate to opposite power modulations.

In support for its inhibitory role, we show that similarly to alpha, decreases in prefrontal and occipitoparietal beta power are contingent upon the occurrence of the informative cue, and associated with faster responses. This is in line with previous reports on the alpha-like gating role played by beta oscillations (Bastos et al., 2018; Miller et al., 2018; van Ede et al., 2011). Interestingly, while there is overlap in functionality and temporal patterns between alpha and beta, the localization of the inhibitory beta effects extends more towards frontoparietal regions, relative to that of the alpha effects.

In support for its circuit role, we demonstrate that increases (rather than decreases) in beta power index a stronger decoding and maintenance of task-relevant features, i.e., the decodability of stimuli preceded by high beta power was boosted and generalized for longer durations. This is in line with previous studies demonstrating that beta power correlates with stimulus information maintained in working memory as well as subsequent decision outcomes (Haegens et al., 2017; Lautz et al., 2017; Proskovec et al., 2019). Here we go one step further, by directly linking the power of beta oscillations to the quality of information content in neural activity patterns. We posit that stronger beta synchronization indexes a stronger (longer lasting) setting up of task-relevant circuits (i.e., working-memory nodes). In turn, this enhanced circuit recruitment leads to more efficient maintenance of stimulus features and thus allows them to be decoded for longer durations.

Taken together, our results corroborate the proposed dual roles for beta rhythms in our framework (Miller et al., 2018; Spitzer & Haegens, 2017). Future invasive studies are required to dissociate the underlying generators (e.g., on the cell circuit/laminar level) of these proposed dual betas. In addition, the temporal and spatial evolution of alpha and beta rhythms should be thoroughly compared, in order to highlight potential differences and similarities in their roles in active inhibition.

4.4 Conclusion

In summary, we demonstrate how rhythms from the delta to beta range might subserve higher-level cognitive functions by providing low-level mechanistic operations. Combined, these oscillatory building blocks allow for selective sampling of input, disengaging and engaging task-irrelevant and relevant networks, and temporal organization of these respective dynamics. Critically, we find that these oscillatory dynamics correlate both with the behavioral performance of the participant, and with the information content in the recorded brain signal.

5 Acknowledgements

References

Axmacher, N., Henseler, M. M., Jensen, O., Weinreich, I., Elger, C. E., & Fell, J. (2010). Cross-frequency coupling supports multi-item working memory in the human hippocampus. *Proceedings of the National Academy of Sciences*, *107*(7), 3228–3233. https://doi.org/10.1073/pnas.0911531107

Bahmani, Z., Daliri, M. R., Merrikhi, Y., Clark, K., & Noudoost, B. (2018). Working Memory Enhances Cortical Representations via Spatially Specific Coordination of Spike Times. *Neuron*, *97*(4), 967-979.e6. https://doi.org/10.1016/j.neuron.2018.01.012

Bahramisharif, A., Jensen, O., Jacobs, J., & Lisman, J. (2018). Serial representation of items during working memory maintenance at letter-selective cortical sites. *PLoS Biology*, *16*(8), e2003805. https://doi.org/10.1371/journal.pbio.2003805

Barne, L. C., Lange, F. P. de, & Cravo, A. M. (2020). Prestimulus alpha power is related to the strength of stimulus representation. *Cortex*, *132*, 250–257. https://doi.org/10.1016/j.cortex.2020.08.017

Bastos, A. M., Loonis, R., Kornblith, S., Lundqvist, M., & Miller, E. K. (2018). Laminar recordings in frontal cortex suggest distinct layers for maintenance and control of working memory. *Proceedings of the National Academy of Sciences*, *115*(5), 1117–1122. https://doi.org/10.1073/pnas.1710323115

Bates, D., Mächler, M., Bolker, B., & Walker, S. (2015). Fitting Linear Mixed-Effects Models Using lme4. *Journal of Statistical Software*, *67*(1). https://doi.org/10.18637/jss.v067.i01

Berger, B., Griesmayr, B., Minarik, T., Biel, A. L., Pinal, D., Sterr, A., & Sauseng, P. (2019). Dynamic regulation of interregional cortical communication by slow brain oscillations during working memory. *Nature Communications*, *10*(1), 4242. https://doi.org/10.1038/s41467-019-12057-0

Bidet-Caulet, A., Bottemanne, L., Fonteneau, C., Giard, M.-H., & Bertrand, O. (2015). Brain Dynamics of Distractibility: Interaction Between Top-Down and Bottom-Up Mechanisms of Auditory Attention. *Brain Topography*, *28*(3), 423–436. https://doi.org/10.1007/s10548-014-0354-x

Bishop, G. H. (1932). Cyclic changes in excitability of the optic pathway of the rabbit. *American Journal of Physiology-Legacy Content*, *103*(1), 213–224. https://doi.org/10.1152/ajplegacy.1932.103.1.213

Breska, A., & Deouell, L. Y. (2017). Neural mechanisms of rhythm-based temporal prediction: Delta phase-locking reflects temporal predictability but not rhythmic entrainment. *PLoS Biology*, *15*(2), e2001665. https://doi.org/10.1371/journal.pbio.2001665

Brunia, C. H. M., & Boxtel, G. J. M. van. (2001). Wait and see. *International Journal of Psychophysiology*, *43*(1), 59–75. https://doi.org/10.1016/s0167-8760(01)00179-9

Busch, N. A., Dubois, J., & VanRullen, R. (2009). The Phase of Ongoing EEG Oscillations Predicts Visual Perception. *The Journal of Neuroscience*, *29*(24), 7869–7876. https://doi.org/10.1523/jneurosci.0113-09.2009

Buzsaki, G. (2006). *Rhythms of the Brain*. Oxford University Press.

Canolty, R. T., Ganguly, K., Kennerley, S. W., Cadieu, C. F., Koepsell, K., Wallis, J. D., & Carmena, J. M. (2010). Oscillatory phase coupling coordinates anatomically dispersed functional cell assemblies. *Proceedings of the National Academy of Sciences*, *107*(40), 17356–17361. https://doi.org/10.1073/pnas.1008306107

Colgin, L. L. (2012). Mechanisms and Functions of Theta Rhythms. *Annual Review of Neuroscience*, *36*(1), 295–312. https://doi.org/10.1146/annurev-neuro-062012-170330

Combrisson, E., Nest, T., Brovelli, A., Ince, R. A. A., Soto, J. L., Guillot, A., & Jerbi, K. (2020). Tensorpac: an open-source Python toolbox for tensor-based Phase-Amplitude Coupling measurement in electrophysiological brain signals. *BioRxiv*, 2020.04.17.045997. https://doi.org/10.1101/2020.04.17.045997

Costers, L., Schependom, J. V., Laton, J., Baijot, J., Sjøgård, M., Wens, V., Tiège, X. D., Goldman, S., D'Haeseleer, M., D'hooghe, M. B., Woolrich, M., & Nagels, G. (2020). Spatiotemporal and spectral dynamics of multi-item working memory as revealed by the n-back task using MEG. *Human Brain Mapping*. https://doi.org/10.1002/hbm.24955

Coull, J. T., & Nobre, A. C. (1998). Where and When to Pay Attention: The Neural Systems for Directing Attention to Spatial Locations and to Time Intervals as Revealed by Both PET and fMRI. *Journal of Neuroscience*, *18*(18), 7426–7435. https://doi.org/10.1523/jneurosci.18-18-07426.1998

Dugué, L., Marque, P., & VanRullen, R. (2015). Theta Oscillations Modulate Attentional Search Performance Periodically. *Journal of Cognitive Neuroscience*, *27*(5), 945–958. https://doi.org/10.1162/jocn_a_00755

ElShafei, H. A., Bouet, R., Bertrand, O., & Bidet-Caulet, A. (2018). Two Sides of the Same Coin: Distinct Sub-Bands in the Alpha Rhythm Reflect Facilitation and Suppression Mechanisms during Auditory Anticipatory Attention. *Eneuro*, *5*(4), ENEURO.0141-18.2018. https://doi.org/10.1523/eneuro.0141-18.2018

Fiebelkorn, I. C., & Kastner, S. (2018). A Rhythmic Theory of Attention. *Trends in Cognitive Sciences*, *23*(2), 87–101. https://doi.org/10.1016/j.tics.2018.11.009

Fiebelkorn, I. C., Saalmann, Y. B., & Kastner, S. (2013). Rhythmic Sampling within and between Objects despite Sustained Attention at a Cued Location. *Current Biology*, *23*(24), 2553–2558. https://doi.org/10.1016/j.cub.2013.10.063

Gramfort, A., Luessi, M., Larson, E., Engemann, D. A., Strohmeier, D., Brodbeck, C., Goj, R., Jas, M., Brooks, T., Parkkonen, L., & Hämäläinen, M. (2013). MEG and EEG data analysis with MNE-Python. *Frontiers in Neuroscience*, *7*, 267. https://doi.org/10.3389/fnins.2013.00267

Griffiths, Benjamin James, Mayhew, S. D., Mullinger, K. J., Jorge, J., Charest, I., Wimber, M., & Hanslmayr, S. (2019). Alpha/beta power decreases track the fidelity of stimulus-specific information. *ELife*, *8*, e49562. https://doi.org/10.7554/elife.49562

Gross, J., Kujala, J., Hamalainen, M., Timmermann, L., Schnitzler, A., & Salmelin, R. (2001). Dynamic imaging of coherent sources: Studying neural interactions in the human brain. *Proceedings of the National Academy of Sciences*, *98*(2), 694–699. https://doi.org/10.1073/pnas.98.2.694

Gudi-Mindermann, H., Rimmele, J. M., Bruns, P., Kloosterman, N. A., Donner, T. H., Engel, A. K., & Röder, B. (2020). Post-training Load-Related Changes of Auditory Working Memory – An EEG Study. *Frontiers in Human Neuroscience*, *14*, 72. https://doi.org/10.3389/fnhum.2020.00072

Gwilliams, L., & King, J.R. (2020). Recurrent processes support a cascade of hierarchical decisions. *ELife*, *9*, e56603. https://doi.org/10.7554/elife.56603

Haegens, S., Cousijn, H., Wallis, G., Harrison, P. J., & Nobre, A. C. (2014). Inter- and intra-individual variability in alpha peak frequency. *NeuroImage*, *92*, 46–55. https://doi.org/10.1016/j.neuroimage.2014.01.049

Haegens, S., Luther, L., & Jensen, O. (2012). Somatosensory Anticipatory Alpha Activity Increases to Suppress Distracting Input. *Journal of Cognitive Neuroscience*, *24*(3), 677–685. https://doi.org/10.1162/jocn_a_00164

Haegens, S., Osipova, D., Oostenveld, R., & Jensen, O. (2010). Somatosensory working memory performance in humans depends on both engagement and disengagement of regions in a distributed network. *Human Brain Mapping*, *31*(1), 26–35. https://doi.org/10.1002/hbm.20842

Haegens, S., Vergara, J., Rossi-Pool, R., Lemus, L., & Romo, R. (2017). Beta oscillations reflect supramodal information during perceptual judgment. *Proceedings of the National Academy*

of Sciences of the United States of America, 114(52), 13810–13815.
https://doi.org/10.1073/pnas.1714633115

Hanslmayr, S., Gross, J., Klimesch, W., & Shapiro, K. L. (2011). The role of alpha oscillations in temporal attention. *Brain Research Reviews, 67*(1–2), 331–343.
https://doi.org/10.1016/j.brainresrev.2011.04.002

Helfrich, R. F., Breska, A., & Knight, R. T. (2019). Neural entrainment and network resonance in support of top-down guided attention. *Current Opinion in Psychology, 29*, 82–89.
https://doi.org/10.1016/j.copsyc.2018.12.016

Henry, M. J., Herrmann, B., & Obleser, J. (2016). Neural Microstates Govern Perception of Auditory Input without Rhythmic Structure. *The Journal of Neuroscience, 36*(3), 860–871.
https://doi.org/10.1523/jneurosci.2191-15.2016

Herbst, S. K., & Landau, A. N. (2016). Rhythms for cognition: the case of temporal processing. *Current Opinion in Behavioral Sciences, 8*, 85–93.
https://doi.org/10.1016/j.cobeha.2016.01.014

Herbst, S. K., & Obleser, J. (2019). Implicit temporal predictability enhances pitch discrimination sensitivity and biases the phase of delta oscillations in auditory cortex. *NeuroImage, 203*, 116198. https://doi.org/10.1016/j.neuroimage.2019.116198

Herding, J., Spitzer, B., & Blankenburg, F. (2016). Upper Beta Band Oscillations in Human Premotor Cortex Encode Subjective Choices in a Vibrotactile Comparison Task. *Journal of Cognitive Neuroscience, 28*(5), 668–679. https://doi.org/10.1162/jocn_a_00932

Hsieh, L.T., Ekstrom, A. D., & Ranganath, C. (2011). Neural Oscillations Associated with Item and Temporal Order Maintenance in Working Memory. *The Journal of Neuroscience, 31*(30), 10803–10810. https://doi.org/10.1523/jneurosci.0828-11.2011

Iemi, L., Busch, N. A., Laudini, A., Haegens, S., Samaha, J., Villringer, A., & Nikulin, V. V. (2019). Multiple mechanisms link prestimulus neural oscillations to sensory responses. *ELife, 8*, e43620. https://doi.org/10.7554/elife.43620

Jensen, O., & Mazaheri, A. (2010). Shaping functional architecture by oscillatory alpha activity: gating by inhibition. *Frontiers in Human Neuroscience, 4*, 186.
https://doi.org/10.3389/fnhum.2010.00186

Jensen, O., & Tesche, C. D. (2002). Frontal theta activity in humans increases with memory load in a working memory task. *European Journal of Neuroscience, 15*(8), 1395–1399.
https://doi.org/10.1046/j.1460-9568.2002.01975.x

Jiang, H., Gerven, M. A. J. van, & Jensen, O. (2015). Modality-specific Alpha Modulations Facilitate Long-term Memory Encoding in the Presence of Distracters. *Journal of Cognitive Neuroscience, 27*(3), 583–592. https://doi.org/10.1162/jocn_a_00726

Jung, T.P., Makeig, S., McKeown, M. J., Bell, A. J., Lee, T.W., & Sejnowski, T. J. (2001). Imaging brain dynamics using independent component analysis. *Proceedings of the IEEE, 89*(7), 1107–1122. https://doi.org/10.1109/5.939827

Kayser, S. J., McNair, S. W., & Kayser, C. (2016). Prestimulus influences on auditory perception from sensory representations and decision processes. *Proceedings of the National Academy of Sciences, 113*(17), 4842–4847. https://doi.org/10.1073/pnas.1524087113

King, J.R., Pescetelli, N., & Dehaene, S. (2016). Brain Mechanisms Underlying the Brief Maintenance of Seen and Unseen Sensory Information. *Neuron, 92*(5), 1122–1134. https://doi.org/10.1016/j.neuron.2016.10.051

King, J.R., & Dehaene, S. (2014). Characterizing the dynamics of mental representations: the temporal generalization method. *Trends in Cognitive Sciences, 18*(4), 203–210. https://doi.org/10.1016/j.tics.2014.01.002

Klimesch, W. (1999). EEG alpha and theta oscillations reflect cognitive and memory performance: a review and analysis. *Brain Research Reviews, 29*(2–3), 169–195. https://doi.org/10.1016/s0165-0173(98)00056-3

Klimesch, W., Sauseng, P., & Hanslmayr, S. (2007). EEG alpha oscillations: The inhibition–timing hypothesis. *Brain Research Reviews, 53*(1), 63–88. https://doi.org/10.1016/j.brainresrev.2006.06.003

Klimesch, W., Schack, B., & Sauseng, P. (2005). The Functional Significance of Theta and Upper Alpha Oscillations. *Experimental Psychology, 52*(2), 99–108. https://doi.org/10.1027/1618-3169.52.2.99

Landau, A. N., & Fries, P. (2012). Attention Samples Stimuli Rhythmically. *Current Biology, 22*(11), 1000–1004. https://doi.org/10.1016/j.cub.2012.03.054

Lautz, A. H. von, Herding, J., Ludwig, S., Nierhaus, T., Maess, B., Villringer, A., & Blankenburg, F. (2017). Gamma and Beta Oscillations in Human MEG Encode the Contents of Vibrotactile Working Memory. *Frontiers in Human Neuroscience, 11*, 576. https://doi.org/10.3389/fnhum.2017.00576

Linkenkaer-Hansen, K., Nikulin, V. V., Palva, S., Ilmoniemi, R. J., & Palva, J. M. (2004). Prestimulus Oscillations Enhance Psychophysical Performance in Humans. *The Journal of Neuroscience, 24*(45), 10186–10190. https://doi.org/10.1523/jneurosci.2584-04.2004

Lundqvist, M., Rose, J., Herman, P., Brincat, S. L., Buschman, T. J., & Miller, E. K. (2016). Gamma and Beta Bursts Underlie Working Memory. *Neuron*, *90*(1), 152–164. https://doi.org/10.1016/j.neuron.2016.02.028

Mazaheri, A., Schouwenburg, M. R. van, Dimitrijevic, A., Denys, D., Cools, R., & Jensen, O. (2014). Region-specific modulations in oscillatory alpha activity serve to facilitate processing in the visual and auditory modalities. *NeuroImage*, *87*, 356–362. https://doi.org/10.1016/j.neuroimage.2013.10.052

Miller, E. K., Lundqvist, M., & Bastos, A. M. (2018). Working Memory 2.0. *Neuron*, *100*(2), 463–475. https://doi.org/10.1016/j.neuron.2018.09.023

Miniussi, C., Wilding, E. L., Coull, J. T., & Nobre, A. C. (1999). Orienting attention in time: Modulation of brain potentials. *Brain*, *122*(8), 1507–1518. https://doi.org/10.1093/brain/122.8.1507

Mitra, P. P., & Pesaran, B. (1999). Analysis of Dynamic Brain Imaging Data. *Biophysical Journal*, *76*(2), 691–708. https://doi.org/10.1016/s0006-3495(99)77236-x

Nobre, A., Correa, A., & Coull, J. (2007). The hazards of time. *Current Opinion in Neurobiology*, *17*(4), 465–470. https://doi.org/10.1016/j.conb.2007.07.006

Nolte, G. (2003). The magnetic lead field theorem in the quasi-static approximation and its use for magnetoencephalography forward calculation in realistic volume conductors. *Physics in Medicine and Biology*, *48*(22), 3637–3652. https://doi.org/10.1088/0031-9155/48/22/002

Oostenveld, R., Fries, P., Maris, E., & Schoffelen, J.-M. (2010). FieldTrip: Open source software for advanced analysis of MEG, EEG, and invasive electrophysiological data. *Computational Intelligence and Neuroscience*, *2011*, 156869. https://doi.org/10.1155/2011/156869

Pedregosa, F., Varoquaux, G., Gramfort, A., Michel, V., Thirion, B., Grisel, O., Blondel, M., Müller, A., Nothman, J., Louppe, G., Prettenhofer, P., Weiss, R., Dubourg, V., Vanderplas, J., Passos, A., Cournapeau, D., Brucher, M., Perrot, M., & Duchesnay, É. (2012). Scikit-learn: Machine Learning in Python. *The Journal of Machine Learning research*, 12, 2825-2830.

Proskovec, A. L., Wiesman, A. I., Heinrichs-Graham, E., & Wilson, T. W. (2019). Load effects on spatial working memory performance are linked to distributed alpha and beta oscillations. *Human Brain Mapping*, *40*(12), 3682–3689. https://doi.org/10.1002/hbm.24625

Puszta, A., Pertich, Á., Giricz, Z., Nyujtó, D., Bodosi, B., Eördegh, G., & Nagy, A. (2020). Predicting Stimulus Modality and Working Memory Load During Visual- and Audiovisual-Acquired

Equivalence Learning. *Frontiers in Human Neuroscience*, *14*, 569142. https://doi.org/10.3389/fnhum.2020.569142

Rohenkohl, G., & Nobre, A. C. (2011). Alpha Oscillations Related to Anticipatory Attention Follow Temporal Expectations. *The Journal of Neuroscience*, *31*(40), 14076–14084. https://doi.org/10.1523/jneurosci.3387-11.2011

Salazar, R. F., Dotson, N. M., Bressler, S. L., & Gray, C. M. (2012). Content-specific fronto-parietal synchronization during visual working memory. *Science*, *338*(6110), 1097–1100. https://doi.org/10.1126/science.1224000

Samaha, J., Iemi, L., & Postle, B. R. (2017). Prestimulus alpha-band power biases visual discrimination confidence, but not accuracy. *Consciousness and Cognition*, *54*, 47–55. https://doi.org/10.1016/j.concog.2017.02.005

Sauseng, P., Griesmayr, B., Freunberger, R., & Klimesch, W. (2010). Control mechanisms in working memory: A possible function of EEG theta oscillations. *Neuroscience & Biobehavioral Reviews*, *34*(7), 1015–1022. https://doi.org/10.1016/j.neubiorev.2009.12.006

Sauseng, P., Peylo, C., Biel, A. L., Friedrich, E. V. C., & Romberg-Taylor, C. (2019). Does cross-frequency phase coupling of oscillatory brain activity contribute to a better understanding of visual working memory? *British Journal of Psychology*, *110*(2), 245–255. https://doi.org/10.1111/bjop.12340

Searle, S. R., Speed, F. M., & Milliken, G. A. (1980). Population Marginal Means in the Linear Model: An Alternative to Least Squares Means. *The American Statistician*, *34*(4), 216–221. https://doi.org/10.1080/00031305.1980.10483031

Singer, W. (1999). Neuronal Synchrony: A Versatile Code for the Definition of Relations? *Neuron*, *24*(1), 49–65. https://doi.org/10.1016/s0896-6273(00)80821-1

Spitzer, B., & Haegens, S. (2017). Beyond the Status Quo: A Role for Beta Oscillations in Endogenous Content (Re)Activation. *Eneuro*, *4*(4), ENEURO.0170-17.2017. https://doi.org/10.1523/eneuro.0170-17.2017

Stolk, A., Todorovic, A., Schoffelen, J.-M., & Oostenveld, R. (2012). Online and offline tools for head movement compensation in MEG. *NeuroImage*, *68*, 39–48. https://doi.org/10.1016/j.neuroimage.2012.11.047

Tallon-Baudry, C., Bertrand, O., Delpuech, C., & Pernier, J. (1996). Stimulus Specificity of Phase-Locked and Non-Phase-Locked 40 Hz Visual Responses in Human. *Journal of Neuroscience*, *16*(13), 4240–4249. https://doi.org/10.1523/jneurosci.16-13-04240.1996

Team, R. C. (2013). *R: A language and environment for statistical computing*.

Thut, G., Nietzel, A., Brandt, S. A., & Pascual-Leone, A. (2006). α-Band Electroencephalographic Activity over Occipital Cortex Indexes Visuospatial Attention Bias and Predicts Visual Target Detection. *The Journal of Neuroscience*, *26*(37), 9494–9502. https://doi.org/10.1523/jneurosci.0875-06.2006

van der Meij, R., Kahana, M., & Maris, E. (2012). Phase–Amplitude Coupling in Human Electrocorticography Is Spatially Distributed and Phase Diverse. *The Journal of Neuroscience*, *32*(1), 111–123. https://doi.org/10.1523/jneurosci.4816-11.2012

van Diepen, R. M., Cohen, M. X., Denys, D., & Mazaheri, A. (2015). Attention and Temporal Expectations Modulate Power, Not Phase, of Ongoing Alpha Oscillations. *Journal of Cognitive Neuroscience*, *27*(8), 1573–1586. https://doi.org/10.1162/jocn_a_00803

van Dijk, H. van, Schoffelen, J.-M., Oostenveld, R., & Jensen, O. (2008). Prestimulus Oscillatory Activity in the Alpha Band Predicts Visual Discrimination Ability. *The Journal of Neuroscience*, *28*(8), 1816–1823. https://doi.org/10.1523/jneurosci.1853-07.2008

van Ede, F., Chekroud, S. R., Stokes, M. G., & Nobre, A. C. (2018). Decoding the influence of anticipatory states on visual perception in the presence of temporal distractors. *Nature Communications*, *9*(1), 1449. https://doi.org/10.1038/s41467-018-03960-z

van Ede, F., Lange, F. de, Jensen, O., & Maris, E. (2011). Orienting Attention to an Upcoming Tactile Event Involves a Spatially and Temporally Specific Modulation of Sensorimotor Alpha- and Beta-Band Oscillations. *The Journal of Neuroscience*, *31*(6), 2016–2024. https://doi.org/10.1523/jneurosci.5630-10.2011

van Ede, F., Niklaus, M., & Nobre, A. C. (2017). Temporal Expectations Guide Dynamic Prioritization in Visual Working Memory through Attenuated α Oscillations. *The Journal of Neuroscience: The Official Journal of the Society for Neuroscience*, *37*(2), 437–445. https://doi.org/10.1523/jneurosci.2272-16.2017

VanRullen, R., Busch, N. A., Drewes, J., & Dubois, J. (2011). Ongoing EEG Phase as a Trial-by-Trial Predictor of Perceptual and Attentional Variability. *Frontiers in Psychology*, *2*, 60. https://doi.org/10.3389/fpsyg.2011.00060

VanRullen, R. (2016). Perceptual Cycles. *Trends in Cognitive Sciences*, *20*(10), 723–735. https://doi.org/10.1016/j.tics.2016.07.006

Van Veen, B. D., Drongelen, W. V., Yuchtman, M., & Suzuki, A. (1997). Localization of brain electrical activity via linearly constrained minimum variance spatial filtering. *IEEE Transactions on Biomedical Engineering*, *44*(9), 867–880. https://doi.org/10.1109/10.623056

Varela, F., Lachaux, J.-P., Rodriguez, E., & Martinerie, J. (2001). The brainweb: Phase synchronization and large-scale integration. *Nature Reviews Neuroscience*, *2*(4), 229–239. https://doi.org/10.1038/35067550

Wang, X.J. (2010). Neurophysiological and Computational Principles of Cortical Rhythms in Cognition. *Physiological Reviews*, *90*(3), 1195–1268. https://doi.org/10.1152/physrev.00035.2008

Yu, X., Chen, Y., Qiu, J., Li, X., & Huang, X. (2017). Neural oscillations associated with auditory duration maintenance in working memory. *Scientific Reports*, *7*(1), 5695. https://doi.org/10.1038/s41598-017-06078-2

Zion Golumbic, E. M., Ding, N., Bickel, S., Lakatos, P., Schevon, C. A., McKhann, G. M., Goodman, R. R., Emerson, R., Mehta, A. D., Simon, J. Z., Poeppel, D., & Schroeder, C. E. (2013). Mechanisms Underlying Selective Neuronal Tracking of Attended Speech at a "Cocktail Party." *Neuron*, *77*(5), 980–991. https://doi.org/10.1016/j.neuron.2012.12.037